Available online at www.sciencedirect.com

ScienceDirect

Procedia Structural Integrity 21 (2019) 130–137

Structural Integrity Procedia

www.elsevier.com/locate/procedia

1st International Workshop on Plasticity, Damage and Fracture of Engineering Materials

3D Simulation of Dynamic Delamination in Curved Composite Laminates

Tamer Tahir Ata[a,b], Demirkan Coker[a,*]

[a]*Middle East Technical University, Department of Aerospace Engineering, Ankara 06800, Turkey*
[b]*Turkish Aerospace Industries (TAI), Ankara 06980, Turkey*

Abstract

In this study, dynamic fracture of curved carbon fiber reinforced plastic (CFRP) laminates under quasi-static loading is investigated using explicit three dimensional (3D) finite element method in conjunction with Cohesive Zone Modelling (CZM). The simulations are based on the experimental studies conducted by Tasdemir (2018). Three dimensional finite element models of two different ply architectures (unidirectional and fabric laminate) are generated corresponding to the experimental configurations. The computational results show good correlation with the experimental results in which a major delamination is observed approximately at 35% of the thickness for both unidirectional and fabric curved laminates. It is also observed that delamination initiates at the half width of the laminate for both specimen configurations. For the fabric laminate, it is interesting to observe that the delamination initiates at the center of the width instead of the free-edges where a material mismatch exists between different layer orientations (Cao et al., 2019; Lagunegrand et al., 2006; Solis et al., 2018). Finite element analysis results are consistent with experiments in terms of main delamination location in thickness direction.

Peer-review under responsibility of the 1st International Workshop on Plasticity, Damage and Fracture of Engineering Materials organizers

Keywords: Delamination; Cohesive Zone Modelling; Dynamic Fracture

* Corresponding author. Tel.: +9-0312-210-4253; fax: +9-0312-210-4250.
E-mail address: coker@metu.edu.tr

Peer-review under responsibility of the 1st International Workshop on Plasticity, Damage and Fracture of Engineering Materials organizers
10.1016/j.prostr.2019.12.094

1. Introduction

Most of the primary and secondary structures include curved shape parts in the aircraft and wind turbine structures. Due to the presence of curved regions at which significant interlaminar stresses are developed, delamination followed by a reduced load carrying capability of the component may cause catastrophic failure of the whole structure. Therefore, it is important to understand the mechanisms of delamination in curved laminated composites.

One of the pioneering studies on delamination in curved laminated composites was performed by Chang and Springer (1986) in which the in-plane failure is predicted using the Tsai-Hill criterion whilst out-of-plane failure is predicted by a quadratic stress criterion proposed by the authors. Sun and Kelly (1988) investigated two possible failure modes (matrix cracking and delamination) of composite angle structures through experimentation and analysis. They concluded that the initial delamination crack growth is unstable. In the early 1990's, Martin (1992) worked on unstable delamination in unidirectional curved composite laminates under quasi-static loading both experimentally and numerically. In 1996, Wisnom (1996) studied the anticlastic curvature in pure bending both in 3D and 2D models assuming generalized plane strain. He addressed the significant variation of stresses across the width of the specimen as a result of the comparison between 3D and 2D models. At the beginning of 2000s, emergence and growth of delamination in L-shaped composite laminates are investigated by Pettermann et al. (2009). They concluded that after a certain delamination size, the delamination propagates in a stable manner. The majority of these investigations on delamination in curved composited were conducted considering the failure process as static. In a series of recent studies, Gozluklu and Coker (2012, 2016) have demonstrated that delamination of L-shaped composite materials is highly dynamic. They performed 2D explicit FEA in conjunction with cohesive zone elements. The dynamic nature of failure of curved beams under quasi-static loading was also shown with experimental studies by Coker and coworkers (Gozluklu et al., 2015; Uyar et al., 2015; Yavas et al., 2014).

In this study, finite element models with cohesive elements at the layer interfaces are generated by using 3D elements in ABAQUS software. The analyses are performed in explicit solver since previous studied revealed that the delamination of L-shaped composite materials is highly dynamic. As a result of the 3D simulations, initial failure location and propagation path of the delamination inside the part are clearly observed.

2. Computational Method

2.1. Material

The material used for unidirectional laminate is AS4/8552 unidirectional prepreg with cured ply thickness of 0.188 mm and density of 1580 kg/m^3. The mechanical and interface properties of this material are provided in Table 1. All other values except interface strengths are directly taken from Camanho et al. (2009). Interface strengths are obtained from experiments (Ata, 2019) conducted according to ASTM Standard D6415 (2006) and ASTM Standard D2344 (2006). The curve fit factor, η, for B-K criterion is taken as 1.45.

Table 1. Mechanical and interface properties of Hexply AS4/8552 UD prepreg and AS4/8552 5HS fabric.

	AS4/8552 UD Prepreg	AS4/8552 5HS Fabric
Elastic Properties	E_{11}=135 GPa; E_{22}= E_{33}=9.6 GPa;	E_{11}= E_{22} =64 GPa; E_{33}=8.5 GPa;
	ν_{12}= ν_{13}=0.32; ν_{23}=0.487	ν_{12}= 0.046; ν_{13}=ν_{23}=0.30
	G_{12}= G_{13}=5.3 GPa; G_{23}=3.4 GPa;	G_{12}= 4.9 GPa; G_{13}=G_{23}=3.7 GPa;
Interface Strength (MPa)	$t_I^0 = 79.07$; $t_{II}^0 = t_{III}^0 = 106.4$	$t_I^0 = 53$; $t_{II}^0 = t_{III}^0 = 79$
Fracture Toughness (N/mm)	$G_{I,C}$=0.28; $G_{II,C}$ = $G_{III,C}$ = 0.79	$G_{I,C}$=0.375;$G_{II,C}$ = $G_{III,C}$ = 1.467

The material used for fabric laminate is AS4/8552 5HS fabric with cured ply thickness of 0.280 mm and density of 1570 kg/m^3. The mechanical and interface properties are provided in Table 1 as done for UD laminate. Mechanical properties are taken from the material specification datasheet (Marlett, 2011). The average of compressive and tensile measured mean values is taken in order to obtain modulus values in warp and weft directions. Interlaminar normal and shear strengths are taken as 53 and 79 MPa, respectively (Hexcel, 2016). Fracture toughness values for each mode are taken from Gozluklu (2014).

The interface stiffnesses of both materials are calculated by using the below given closed-form expression derived by Turon et al. (2007):

$$K = \frac{\alpha E_3}{t} \tag{1}$$

Wave speeds in both AS4/8552 UD Prepreg and AS4/8552 5HS Fabric are calculated using the formulas from Coker et al. (2001) and provided in Table 2.

Table 2. Material wave speeds for AS4/8552 UD prepreg and AS4/8552 5HS fabric.

	$c_l''(m/s)$	$c_l^{\perp}(m/s)$	$c_s(m/s)$	$c_R(m/s)$	$V_c(m/s)$
UD Prepreg	9377	2852	1831	1816	8045
5HS Fabric	6434	6434	1767	1761	6243

2.2. Geometry and Boundary Conditions

The geometry of the curved CFRP laminate is shown schematically in Fig. 1 for both unidirectional and fabric specimens. The upper and lower arm lengths (l) are 66.36 mm. Inner radius (r_i) and width (w) of the considered specimens are 8.0 mm and 25 mm, respectively. The unidirectional laminate, $[\ 0\ ]_{30}$, is composed of 30 unidirectional plies of carbon fiber reinforced plastic with a ply thickness of 0.188 mm which corresponds to 5.64 mm total thickness. The fabric laminate, $[(45/0)_7,45/45/0/45]$, is composed of 18 5HS fabric plies of carbon fiber reinforced plastic with a ply thickness of 0.28 mm which corresponds to a total thickness of 5.04 mm.

Schematic of the experimental configuration (Tasdemir and Coker, 2019) and finite element idealization of load and boundary conditions are shown in Fig. 2. The freely rotating pin and bolts are not considered in the finite element model. This connection and boundary condition case are simulated with kinematic couplings which transfers applied boundary conditions to the specimen from upper and lower load introduction points. The remaining parts of the specimen (from bolt attachment region to free edge) are not modelled since they have no contribution to the stiffness and are far away from the considered curve region. The finite element model of the specimen is allowed to move in the y-direction at the upper load introduction point and rotation around the z-axis is allowed at both upper and lower load introduction points. Allowing rotation around the z-axis accommodates a freely rotating pin clearly. All other degrees of freedom (displacement and rotational degrees of freedom are referred as U and R, respectively) are fixed at both load introduction points. The maximum applied displacement is set to 7 mm and applied at the upper load introduction point as shown below in figure. Load is applied to the specimen with a smooth-step amplitude in order to simulate quasi-static loading.

2.3. Finite Element Model

In the three-dimensional finite element model, the bulk region was modelled by reduced integration continuum solid elements (C3D8R) and interfaces between adjacent layers was modelled by 3D cohesive elements (COH3D8). The three-dimensional finite element model of the unidirectional laminate consists of only one layer of cohesive

elements since only the critical interface predicted by analytical approach is considered. This finite element model includes 936320 linear hexahedral elements of type C3D8R and 46816 linear hexahedral elements of type COH3D8. The total number of elements is 983136 and the total number of nodes is 1043616 with a total of 3130854 degrees of freedom.

The three-dimensional finite element model of the fabric laminate includes 17 interfaces and all of them are modelled with cohesive elements and each solid layer is modelled with only one element. This finite element model includes 874800 linear hexahedral elements of type C3D8R and 826200 linear hexahedral elements of type COH3D8. The total number of elements is 1701000 and the total number of nodes is 1772318 with a total of 5316960 degrees of freedom.

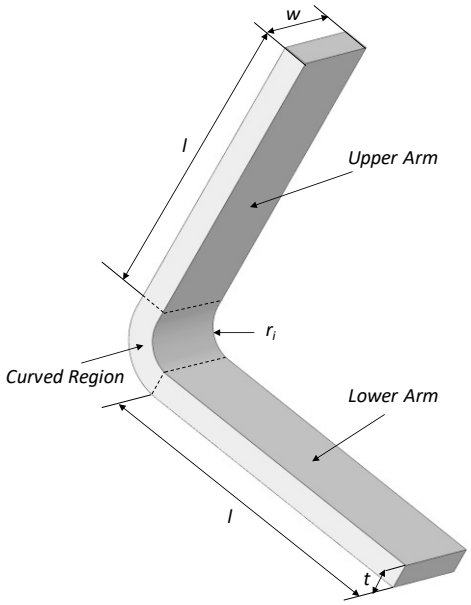

Fig. 1. Specimen geometry.

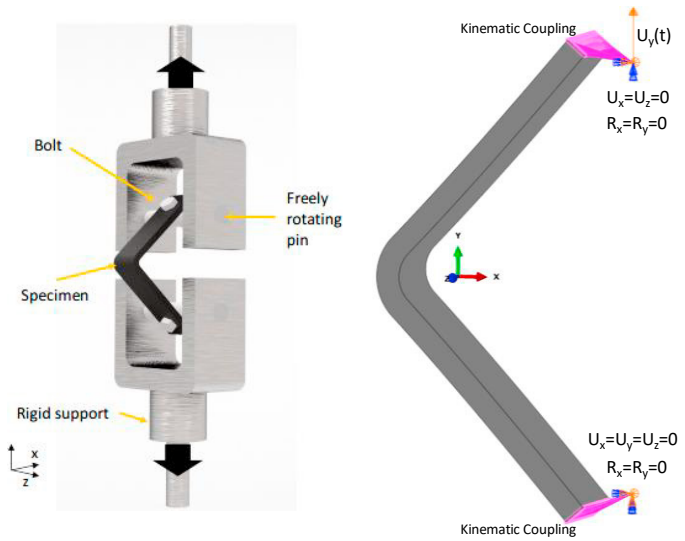

Fig. 2. Schematic of the experimental configuration (Tasdemir and Coker, 2019) and finite element idealization of load and boundary conditions.

2.4. Cohesive Zone Modelling

Local stress goes to infinity in the vicinity of the crack tip according to the theory of elasticity that is why fracture mechanics approach is preferred generally in crack initiation and propagation studies. One of the most common fracture mechanics application is cohesive zone modelling (CZM). In this study, bilinear CZM with quadratic damage initiation criterion is employed. The quadratic nominal stress criterion for mixed-mode loading can be expressed as;

$$f = \left\{ \frac{\langle t_I \rangle}{t_I^0} \right\}^2 + \left\{ \frac{t_{II}}{t_{II}^0} \right\}^2 + \left\{ \frac{t_{III}}{t_{III}^0} \right\}^2 \tag{2}$$

in which t_I, t_{II}, t_{III} are the tractions in each fracture mode as normal, shear, and tearing, respectively. Damage initiates when this equation equals to one. The superscript "0" in denominator of each term is used to express the interfacial strength of that fracture mode. The symbol (< >) used in the normal stress component refers to the Macaulay bracket and it is defined as follow:

$$\langle t_I \rangle = \frac{\left(t_I + |t_I|\right)}{2} \tag{3}$$

As can be understood from the Eqn. 3, the Macaulay bracket in the first term implies that compressive stresses do not cause damage. The interaction between different fracture modes is taken into account both for the onset and propagation of delamination through quadratic nominal stress criterion and Benzeggagh and Kenane (1996) criterion, respectively. The mixed-mode damage propagation criterion is given as;

$$G_{equiv,C} = G_{IC} + \left(G_{IIC} - G_{IC}\right)\left(\frac{G_{II} + G_{III}}{G_I + G_{II} + G_{III}} \right)^{\eta} \tag{4}$$

where G_{IC} and G_{IIC} are the fracture toughness values in Mode-I and Mode-II, respectively. G_I, G_{II}, and G_{III} are the strain energy release rates for each related fracture mode. The parameter (η) is the curve fitting factor obtained from mixed-mode bending (MMB) experiments.

3. Results and Discussion

Fig. 3 represents the evolution of damage in the 12th interface with time after the peak load is attained at which delamination is nucleated in the center of the width in the UD specimen. The shaded areas represent the delamination region inside the specimen. Delamination onset is observed to occur at the center of the width. The delamination then grows in both the transverse (through the width) direction and the longitudinal (along the beam length) direction. When the transverse crack reaches the edge of the specimen at Δt= 11 μs, it nucleates an edge crack that propagates in the longitudinal direction along the beam length. Afterwards, a single crack front which consists of the center and edge cracks propagates along the beam length. At 14 μs from delamination initiation, edge crack reaches the specimen arms where it travels faster than center crack for 12 μs. At Δt= 53 μs, the edge crack begins to slow down and the center crack catches the edge crack after which the crack front moves at a small speed to the end of the specimen arms.

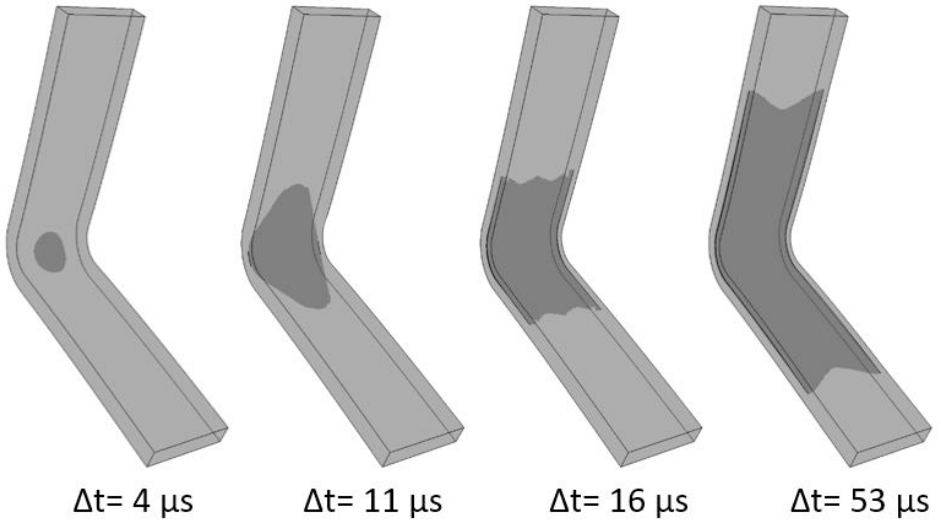

Fig. 3. Delamination propagation path inside the curved unidirectional laminate.

Fig. 4 represents the evolution of damage in the 6th interface with time after the peak load is attained at which delamination is nucleated in the center of the width in the fabric specimen. As before, the shaded areas represent the delamination region inside the specimen. Since elastic property mismatch between plies with different orientations induces stress concentrations near free edges, it is expected that the delamination initiates at the free edge. Contrary to this expectation, delamination initiated at the half-width of the specimen in the same manner as in the unidirectional laminate. Transverse crack reaches the edge at Δt= 19 μs. After 24 μs from delamination initiation, edge crack reaches the end of the curved region and continues to propagate in the specimen arms. The edge crack reaches intersonic speed at the arm region as shown in the next section, it passes the center crack between Δt= 35 μs and Δt= 69 μs. Afterwards, the edge crack slows down, and the center crack catches up with the edge crack moving as a single uniform crack front.

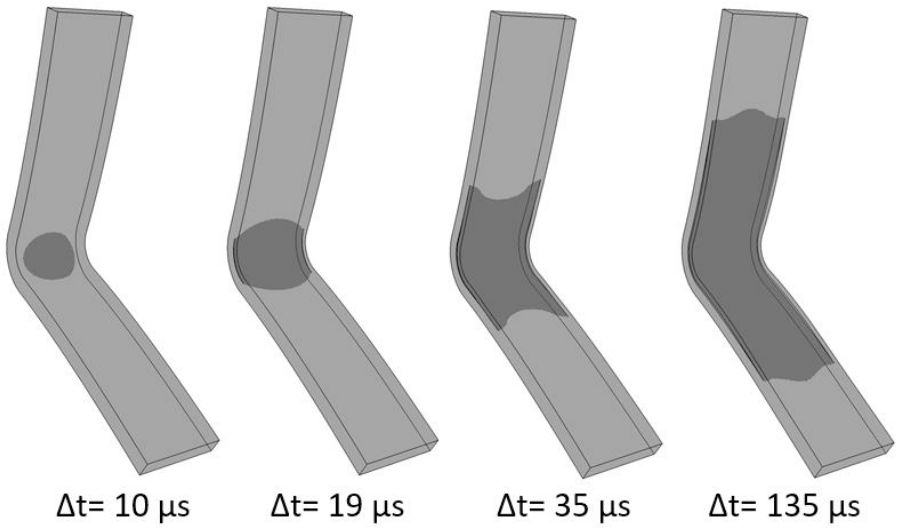

Fig. 4. Delamination propagation path inside the curved fabric laminate.

Variation of edge crack tip speed with respect to time for UD (red circle marker) and fabric (blue square marker) laminates are shown in Fig. 5. The initial time is taken to be the time at the peak load which also corresponds to the initiation of delamination at the center of the width of the specimen. Shear and critical wave speeds are also shown for both UD and fabric laminates. The edge crack in the UD specimen initiates at 11 μs after peak load and reaches a maximum speed of 5500 m/s in 4 μs at the end of curved region (EOCR UD). The crack tip travels at intersonic speeds for 5 μs as it gradually slows down to sub-Rayleigh wave speeds and finally arrests at 30 μs. In the fabric specimen, the edge crack initiates at 16 μs after the peak load. The edge crack attains an intersonic speed of 2400 m/s in 2 μs. Then it decreases to sub-Rayleigh wave speed of approximately 1700 m/s for 2 μs. However, it immediately increases to a maximum crack tip speed of 2700 m/s at the end of the curved region (EOCR Fabric). Afterwards, at the arm region the crack gradually slows down zero crack tip speed in 13 μs. In both cases, the crack initiates under pure Mode-I loading and attain intersonic speeds at the end of the curved region where shear dominated mixed mode loading is observed. This is consistent with the literature where intersonic speeds are observed in composites only under shear dominated loading (Coker and Rosakis, 2001).

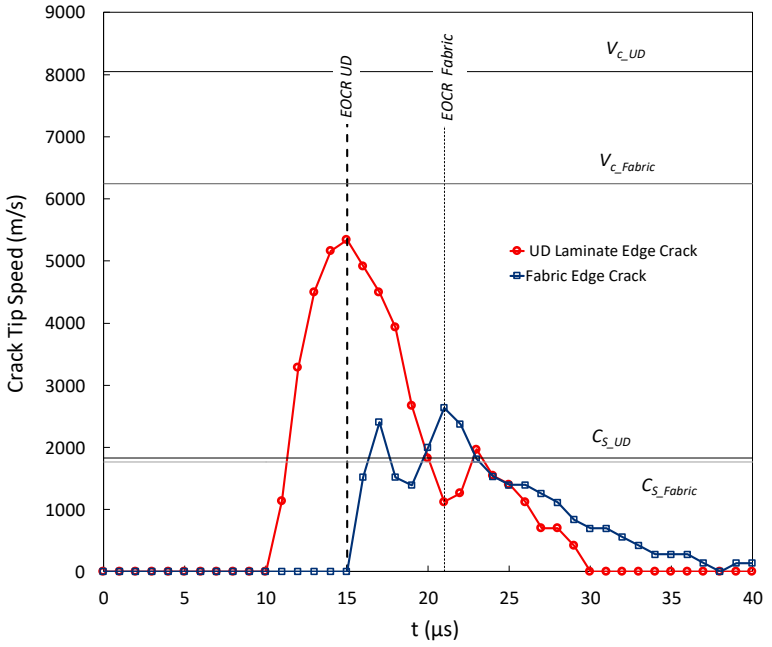

Fig. 5. Edge crack tip speed as a function of time for UD and fabric laminate.

4. Conclusion

In this study, 3D explicit finite element analyses of dynamic delamination in UD ($[0]_{30}$) and fabric ($[(45/0)_7,45/45/0/45]$) curved CFRP laminates are performed under quasi - static loading. The conclusions of this computational study are as follows:

- Delamination nucleates at the center of the width for both specimens and at the interface where the radial stress reaches the maximum value. For the fabric laminate, it is interesting to observe that the delamination initiates at the center of the width instead of the free-edges where a material mismatch exists between different layer orientations (Cao et al., 2019; Lagunegrand et al., 2006; Solis et al., 2018).
- Delamination initiates at sub-Rayleigh wave speeds under Mode-I condition for both UD and Fabric laminates and reaches intersonic speeds as the delamination grows towards the arms.
- For UD laminate, the delamination is initiated at the 12th interface. This location is determined from 2D

analysis results and is in good correlation with the experimental results (Tasdemir, 2018) in which the delamination occurs to initiate approximately at 35% of the thickness from inner radius.

- For fabric laminate, the delamination is initiated at the 6th interface which corresponds to 33% of the thickness from inner radius. This results shows good correlation with the experimental results (Tasdemir, 2018) in which the main delamination is also observed at the 33% of the thickness from inner radius.
- The propagation of delamination in the fabric laminate is slower than the UD laminate.

Acknowledgements

The authors would like to acknowledge to RÜZGEM, METU Center for Wind Energy and Turkish Aerospace Industries (TAI) for their continuous support.

References

ASTM International. Standard D2344 - standard test method for short-beam strength of polymer matrix composite materials. West Conshohocken (PA); 2006. http://dx.doi.org/10.1520/D2344.

ASTM International. Standard D6415 - standard test method for measuring the curved beam strength of a fiber-reinforced. West Conshohocken (PA); 2006. http://dx.doi.org/10.1520/D6415.

Ata, T. T., 2019. 2D and 3D Finite Element Analyses of Dynamic Delamination in Curved CFRP Laminates. MSc thesis, Middle East Tech Univ.

Benzeggagh M.L., Kenane M., 1996. Measurement of mixed-mode delamination fracture toughness of unidirectional glass/epoxy composites with mixed-mode bending apparatus. Compos. Sci. Technol. 56, pp. 439–449.

Cao D., Hu H., Duan Q., Song P., Li S., 2019. Experimental and three-dimensional numerical investigation of matrix cracking and delamination interaction with edge effect of curved composite laminates. Composite Structures 225.

Chang F., Springer G.S., 1986. The strength of fiber reinforced composite bends. Journal of composite materials 20, pp. 30-45.

Coker D., Rosakis A.J., 2001. Experimental observations of intersonic crack growth in asymmetrically loaded unidirectional composite plates. Philosophical Magazine A 81(3), pp. 571-595.

Gozluklu B., Coker D., 2012. Modeling of the dynamic delamination of L-shaped unidirectional laminated composites. Composite Structures 94, pp. 1430-1442.

Gozluklu B., 2014. Modelling of Intersonic Delamination in Curved-Thick Composite Laminates under Quasi-Static Loading, Middle East Technical University.

Gozluklu B., Uyar I., Coker D., 2015. Intersonic delamination in curved thick composite laminates under quasi-static loading. Mechanics of Materials 80, pp. 163-182.

Gozluklu B., Coker D., 2016. Modeling of dynamic crack propagation using rate dependent interface model. Theoretical and Applied Fracture Mechanics 85, pp. 191-206.

Hexcel Corporation, 2016. HexPly 8552 Prod. Data Sheet, pp. 1–6.

Lagunegrand L., Lorriot T., Harry R., Wargnier H., Quenisset J.M., 2006. Initiation of free-edge delamination in composite laminates. Composites Science and Technology 66 (10), pp. 1315-1327.

Lopes C. S., Camanho P. P., Gürdal Z., Maimí P., González E. V., 2009. Low Velocity Impact Damage on Dispersed Stacking Sequence Laminates. Part II: Numerical simulations. Composites Science and Technology 69 (7–8), pp. 937–947.

Marlett K., 2011. Hexcel 8552S AS4 Plain Weave Fabric Prepreg 193 gsm & 38% RC Qualification Material Property Data report. National Institute for Aviation Research, Wichita State University, CAM-RP-20110-006.

Martin R.H., 1992. Delamination failure in a unidirectional curved composite laminate. Composite Materials Testing 10, pp. 365–83.

Solis A., Sánchez-Sáez S., Barbero E., 2018. Influence of ply orientation on free-edge effects in laminates subjected to in-plane loads. Composites Part B: Engineering 153, pp. 149-158.

Sun C.T., Kelly S.R., 1988. Failure in Composite Angle Structures Part I: Initial Failure. Journal of Reinforced Plastics and Composites 7, pp 220-232.

Tasdemir B., Coker D., 2019. Comparison of damage mechanisms in curved composite laminates under static and fatigue loading. Composite Structures 213, pp. 190-203.

Tasdemir, B., 2018. Fatigue and static behavior of curved composite laminates. MSc thesis, Middle East Techn Univ.

Turon A., Davila C.G., Camanho P.P., Costa J., 2007. An engineering solution for mesh size effects in the simulation of delamination using cohesive zone models. Engineering Fracture Mechanics 74, pp. 1665-1682.

Uyar I., Arca M.A., Gozluklu B., Coker D., 2015. Experimental observations of dynamic delamination in curved [0] and [0/90] composite laminates. Fracture, Fatigue, Failure, and Damage Evolution 5, pp. 189-196.

Wimmer G., Kitzmüller W., Pinter G., Wettemann T., Pettermann H.E., 2009. Computational and Experimental Investigation of Delamination in L-shaped Laminated Composite Components. Engineering Fracture Mechanics 76, pp. 2810-2820.

Wisnom M., 1996. 3D finite element analysis of curved beams in bending. J Comp Mater 30, pp. 1178–1190.

Yavas D., Gozluklu B., Coker D., 2014. Investigation of Crack Growth Along Curved Interfaces in L-shaped Composite and Polymers. Fracture and Fatigue 7, pp. 45-50.